Heliyon 10 (2024) e39523

Contents lists available at ScienceDirect

Heliyon

journal homepage: www.cell.com/heliyon

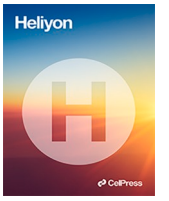

Research article

Analysis of the electrical conductivity and activation energies of bismuth titanate ($Bi_4Ti_3O_{12}$)

Carmen Martínez-Morales [a,*], Paulina Arellanes-Lozada [b], Josué López Rodríguez [a,**], Antonio Romero-Serrano [a], D. González-García [a]

[a] *Instituto Politécnico Nacional, Escuela Superior de Ingeniería Química e Industrias Extractivas, Departamento de Ingeniería en Metalurgia y Materiales, UPALM-Zacatenco, Av. Instituto Politécnico Nacional s/n, Ciudad de México, CP, 07738, Mexico*

[b] *Gerencia de Investigación en Explotación, Instituto Mexicano del Petróleo, Eje Central Lázaro Cárdenas, Col. San Bartolo Atepehuacan, 07738, Mexico City, Mexico*

ARTICLE INFO

Keywords:
Bismuth titanate
Semiconductors
Oxygen partial pressure
Point defects
Electric properties

ABSTRACT

In this study, bismuth titanate ($Bi_4Ti_3O_{12}$) was synthesized from pure solid compounds and structurally characterized by X-ray diffraction (XRD), scanning electron microscopy (SEM), and X-ray photoelectron spectroscopy (XPS). The electrical properties were evaluated by measuring the electrical conductivity of $Bi_4Ti_3O_{12}$ at various oxygen partial pressures ($pO_2 = 10^{-5}$ and 10^{-8} atm) and temperatures (450 °C-750 °C). The electrical conductivity behavior was assessed during the heating and cooling processes. The material activation energies were determined based on the heating curve, which displayed Arrhenius-type behavior and activation energy slope changes, which could be attributed to point defects. When the temperature was increased from 450 °C to 750 °C at oxygen partial pressures $pO_2 = 10^{-5}$ atm, the electrical conductivity increased by about 62.9 %, whereas when the temperature decreased from 750 °C to 450 °C, the electrical conductivity was reduced by 35.95 %. The electrical behavior of $Bi_4Ti_3O_{12}$ was analyzed by establishing its electrical conductivity and chemical activity under different oxygen partial pressures and heating-cooling conditions can allow the synthesis of materials with attractive characteristics for electronic applications.

1. Introduction

In recent decades, ferroelectric ceramics as electronic materials have drawn significant attention as research subject matter due to their applications in capacitors, ultrasound transducers, piezoelectric sensors, non-volatile memories, and ultrasonic motors [1–4]. These materials are known for their high polarization capacity, enabling substantial charge storage [5–7]. The ferroelectric and piezoelectric properties are associated with low-symmetry crystallographic structures, e.g. perovskite-type ferroelectric materials that exhibit spontaneous polarization and can be reoriented between different equilibrium states by applying an electric field [7,8]. Bismuth titanates, originally studied by Aurivillius, constitute an important family of ferroelectric and piezoelectric compounds [9]. These materials belong to the perovskite family and are known as layered bismuth compounds or layered perovskites [10]. Specifically, $Bi_4Ti_3O_{12}$ is a layered perovskite oxide, and its structure consists of alternating various pseudo-perovskite layers $(Bi_2Ti_3O_{10})^{2-}$

* Corresponding author.
** Corresponding author.
E-mail addresses: kar.mtz.m@gmail.com (C. Martínez-Morales), jjlopezr@ipn.mx (J.L. Rodríguez).

https://doi.org/10.1016/j.heliyon.2024.e39523
Received 28 June 2024; Received in revised form 31 August 2024; Accepted 16 October 2024
Available online 18 October 2024

separated by bismuth oxide $(Bi_2O_2)^{2+}$ layers [10,11]. This structure favors platelets growing primarily in the *ab* plane, in which higher electrical conductivity is present [12]. Bismuth titanates have been extensively studied owing to interesting properties such as piezoelectricity, being a less toxic alternative to lead oxide-based electronic devices [11,13]; ferroelectricity for applications in nonvolatile and dynamic computer memories [14]; photocatalytic features, because of their environmentally friendly characteristics [15,16]; and nonlinear optics [14]. This interesting material has shown high electrical strain resistance, i.e. it can be polarized and depolarized multiple times without significantly losing its dielectric properties; it has displayed high spontaneous polarization of approximately 50 μC/cm^2; high ferroelectric Curie temperature ($T_c \sim 670$ °C), as well as high piezoelectric coefficient ($d_{11} = 39$ pC N^{-1}) [4,12,16].

The effect exerted by the structure, pressure, and temperature on the electrical, piezoelectric, and ferroelectric properties has been extensively investigated [17–21]. Such properties can be modified by material composition changes and by introducing point defects or residual stress into the crystal lattice. Unlike mechanical properties, electrical ones are significantly influenced by point crystalline defects that are activated thermally; the concentration of most point defects is controlled by pressure and temperature. In the case of bismuth titanates, oxygen partial pressure (pO_2) plays a major role given its nature [22], as reported by Takahashi et al., who stated that total electrical conductivity in bismuth titanate polycrystalline samples is dependent on pO_2 [23].

The conductivity analysis of ceramic materials allows the identification of conduction mechanisms by activation energies occurring under certain pressure and temperature conditions. The analysis of conduction mechanisms plays an important role in determining applications of semiconductor materials. For example, while in certain applications such as enhancing spontaneous polarization it is desirable to decrease conductivity [24], in transistors it is more important to increase conductivity [25]. Specifically for application of ferroelectric ceramics as capacitors an important problem to be controlled is the high parasitic currents that prevent adequate device polarization. These currents are produced by either holes or free electrons that compensate for defects being out of equilibrium because the rapid tempering or cooling process prevent the defect concentrations from reaching equilibrium [26]. In contrast, bismuth titanate has been proposed as an excellent conductor of oxygen ions due to its chemical characteristics [26]. Highly polarizable Bi^{3+} ions have been reported to provide low diffusion barriers that allow the migration of oxygen ions [27]. The application of $Bi_4Ti_3O_{12}$ in diverse devices depends on defect concentrations and previous studies have been focused on point defects of this material to enhance the performance of various electronic systems, such as transistors. High leakage current and electrical conductivity have been reported to be associated with oxygen vacancies formed during the sintering process [24]. Jeong Yun-Gi et al. evaluated piezoelectricity, thermal stability and fatigue resistance of high-temperature-Nb/Ta-doped $Bi_4Ti_3O_{12}$ piezoceramics, concluding that decreasing oxygen vacancy defects is crucial in improving stability against degradation caused by high temperatures and electric fields [24]. In a previous study, Martínez et al. studied the behavior of $Bi_4Ti_3O_{12}$ point defects and constructed the Brouwer diagram at 650, 800, and 1000 °C, which provided insight into mobility and presence of point defects created under specific pressures and temperatures. Conductivity at 650 °C and 741 °C at different oxygen partial pressures was also reported [28].

The structural modification of $Bi_4Ti_3O_{12}$ by diverse synthesis methods without controlled atmosphere and introducing doping elements into bismuth titanate with different phases has been intensively dealt with [12,29–33]. In contrast, it has been claimed that activation energy measurements at different temperatures help determine point defects in bismuth titanate [12,34]. Shulman et al. studied the microstructure influence on the electrical conductivity and piezoelectric properties of $Bi_4Ti_3O_{12}$, including the effect of a doping element on the conductivity and activation energies at 50 °C-650 °C [35]. Mechanical activity of $Bi_4Ti_3O_{12}$ at 50 °C–650 °C was also researched by Hwee et al. who asserted that activation energy of ~0.1 eV over a temperature interval ranging from 50° to 200 °C was probably due to hole mobility, while at 200°–650 °C, activation energy of ~1.1 eV was related to hole mobility, vacancies, and ionization enthalpy in $Bi_4Ti_3O_{12}$ [36]. Moreover, Ambriz-Vargas et al. studied the effect of point defects on the ferroelectric properties of niobium-doped bismuth titanate, and concluded that the compensation mechanism used by the material to re-establish electrical neutrality is bismuth vacancies at higher Nb concentrations [37].

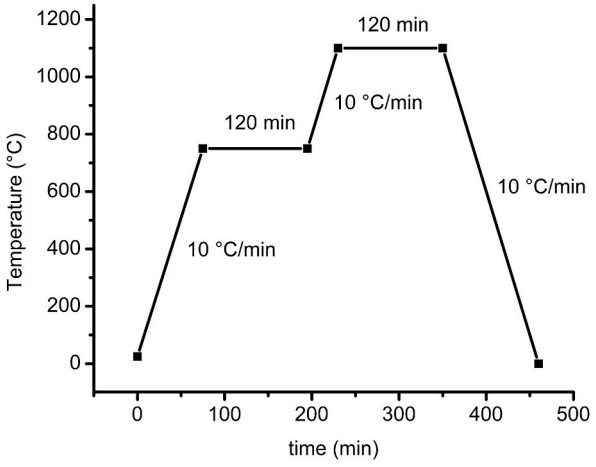

Fig. 1. Heating and cooling ramp for the sintering of $Bi_4Ti_3O_{12}$.

The study of the conductivity behavior as a function of temperature and oxygen partial pressure and its relationship with point defects is yet to be fully explored for potential $Bi_4Ti_3O_{12}$ applications. Therefore, the present study focused on the methods for synthesizing $Bi_4Ti_3O_{12}$ and its characterization by X-Ray Diffraction (XRD), Scanning Electron Microscopy (SEM), and X-ray Photoelectron Spectroscopy (XPS). The electrical properties of $Bi_4Ti_3O_{12}$ were analyzed using the electrical conductivity obtained at different temperatures (450 °C-750 °C) and oxygen partial pressures ($pO_2 = 10^{-5}$ and 10^{-8} atm) during heating and cooling processes. The heating curve slopes determine the material activation energies and establish their relationship with point defects in the synthesized $Bi_4Ti_3O_{12}$.

2. Methods

A solid-state reaction was carried out using the Aldrich analytical grade precursors TiO_2 and Bi_2O_3, heated at 300 °C for 1 h to eliminate humidity. Subsequently, the precursors were weighed and mixed according to the stoichiometric composition. Then, 0.9 g pellets were placed in a platinum crucible, followed by the heating and cooling steps for $Bi_4Ti_3O_{12}$ sintering (Fig. 1). The first step was carried out at the heating rate of 10 °C/min from room temperature up to 750 °C to avoid Bi loss [38]. The system was maintained at this temperature for 2 h under constant stirring. The high thermal stirring of Bi_2O_3 would efficiently react with TiO_2, forming intermediate phases, such as $Bi_4Ti_3O_{12}$, with high melting points [39]. The second heating step was at 10 °C/min up to 1100 °C; this temperature was maintained for 2 h. Finally, the system was cooled to room temperature at 10 °C/min.

The obtained material was characterized by XRD on a Bruker D8 Focus X-ray diffractometer with Cu kα source (λ = 1.54056 Å), using the software DIFFRAC.EVA to produce the spectra. The SEM analysis was conducted using a JEOL 6300 scanning electron microscope at 1000x. The digitization of the SEM micrographs was analyzed

with the image processing software ImageJ v1.51j8 to determine the plate thickness. The XPS assays were carried out using a K-Alpha Thermo Fisher Scientific spectrometer with monochromatic Al Ka to generate high-resolution graphs and spectra (X-ray source of 1486.6 eV). The binding energy scale was calibrated at 285 eV using the C 1s signal related to adventitious carbon layer and background correction was achieved using a Shirley background function.

The electrical conductivity of $Bi_4Ti_3O_{12}$ was measured in a designed device shown in Fig. 2. The principle of this device consists in applying voltage between two electrodes, in which the material resistance is measured and transformed into conductivity. A $Bi_4Ti_3O_{12}$ pellet was held and connected via platinum wires to a multimeter to measure the resistance and determine the conductivity, which is the ability of a material to transmit an electric current through a given distance. The reactor atmosphere contained oxygen with partial pressure of 10^{-5} atm using a N_2/O_2 mixture and 10^{-8} atm employing a N_2/CO_2 mixture. As it is known, electrical conductivity grows in semiconductors with increasing temperature; therefore, the temperature interval ranging from 450 °C to 750 °C was used in the present work. With these temperature changes, electrons from the valence band could jump to the conduction band, creating free motion between the two bands and thus increasing conductivity [40,41].

3. Results and discussion

3.1. XRD, SEM, and XPS characterization

Fig. 3a–b) shows the XRD pattern of $Bi_4Ti_3O_{12}$ before and after conductivity measurements, respectively, where all peaks have been

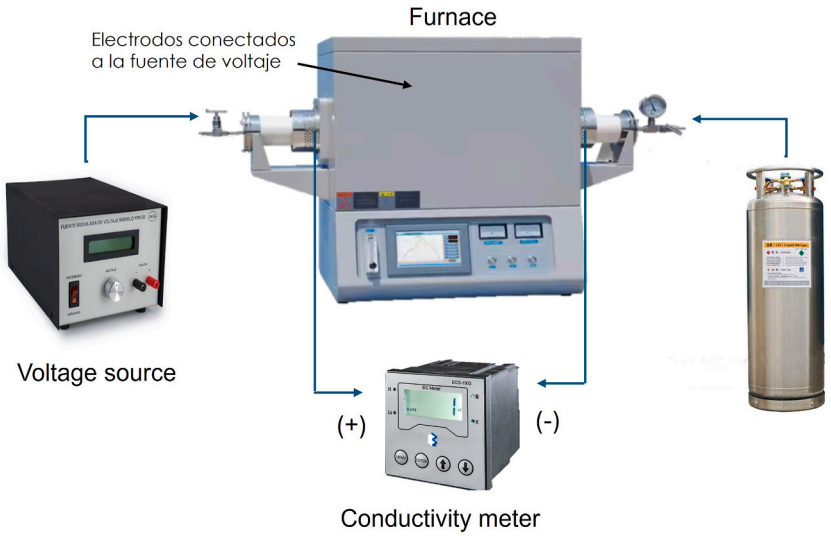

Fig. 2. Arrangement for measuring the electrical conductivity of $Bi_4Ti_3O_{12}$.

indexed according to JCPDS 00-035-0795 card corresponding to $Bi_4Ti_3O_{12}$ (see Fig. 3 c)). The crystal structure of $Bi_4Ti_3O_{12}$ is base-centered orthorhombic, whose lattice parameters are a = 5.44890 Å, b = 32.81500 Å, c = 5.41000 Å, and remain unchanged after heating and cooling process. Fig. 3 b) shows an increase in the intensity of multiple peaks in the diffraction pattern compared to the original sample, which is attributed to a preferential orientation in the corresponding crystallographic planes due to the thermal cycle.

Fig. 4 a) and c) show SEM micrograph of the $Bi_4Ti_3O_{12}$ before and after conductivity measurements, where the presence of randomly distributed elongated plates is observed. This morphology is consistent with other work that studied bismuth titanate [42–44]. Additionally, average thickness of plates before the conductivity measurements was 5.02 μm (Fig. 4 b)), while after the measurements it increases to 6.48 μm (Fig. 4 d)). This slight change is attributed to the crystal grow of bismuth titanate promoted by the temperature increase. Finally, $Bi_4Ti_3O_{12}$ after the conductivity measurements presents a higher number of stacked layers, this could be due to the compressive stress applied to the material, induced by the electrodes during the heating and cooling process.

XPS was used to establish the oxidation state of Bi and Ti. Fig. 5 shows the high-resolution spectra of the Bi 4f, Bi 4d, Ti 2p, and O 1s; and core level binding energy and full width half maximums are summarized in Table 1. Fig. 5a illustrates the Bi 4f spectrum with the characteristic Bi $4f_{7/2}$ and Bi $4f_{5/2}$ components at 159.0 eV and 164.2 eV, respectively, with a shift between the two components of 5.2 eV which is consist with other studies. Indicating the presence of Bi (III) oxides [45–47]. Furthermore, Bi $4d_{3/2}$ becomes evident at the binding energy of 465.6 eV, as shown in Fig. 5b; this region is overlapped with the Ti 2p spectrum. Two characteristic Ti 2p peaks are observed at 458.0 eV and 463.6 eV, corresponding to Ti $2p_{3/2}$ and Ti $2p_{1/2}$, respectively; components shifted by 5.6 eV. These results confirm the presence of Ti (IV) oxides [45–48], the expected oxidation state as reported previously [49–51]. A main peak was observed at 529.6 eV for the O 1s spectrum at high resolution (Fig. 5c), which can be associated with metal-oxygen bonds. The low intensity, secondary peak at 531.4 eV is related to the natural presence of surface hydroxide pollutants and/or O^- adsorbed species at the oxygen vacancy sites [45–48]. The shift between these two peaks is 1.8 eV; in systems in presence of oxides and surface contamination has been reported a similar shift, therefore it is possible confirm these O 1s assignments [46]. In addition, the Bi:Ti:O ratio obtained was 4:3:8.3, the low atomic O/Bi ratio of 2.075 respect to the stoichiometrically expected 3.0, confirms the presence of oxygen vacancies [46]. These point defects might result from Bi volatilization during high-temperature synthesis [45].

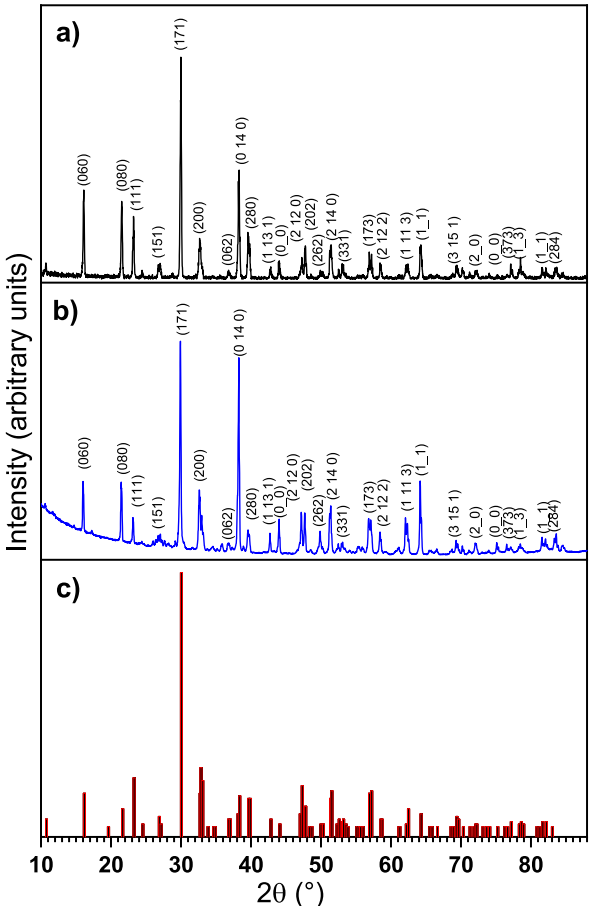

Fig. 3. XRD pattern of $Bi_4Ti_3O_{12}$: a) original, b) after conductivity measurements at $pO_2 = 10^{-8}$ atm, and c) JCPDS 00-035-0795 card.

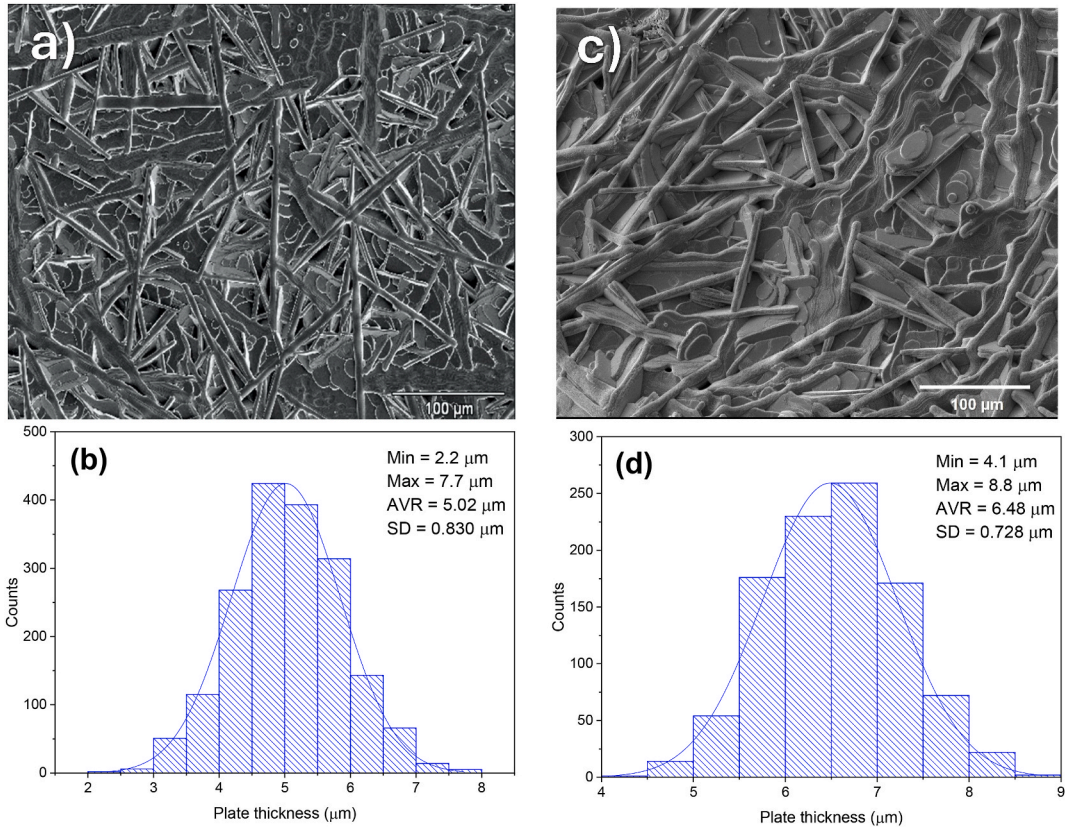

Fig. 4. SEM micrograph and plate thickness distribution histogram of the $Bi_4Ti_3O_{12}$ a-b) before and c-d) after conductivity measurements.

3.2. Conductivity

The conductivity of $Bi_4Ti_3O_{12}$ was measured at different temperatures and oxygen partial pressures. Fig. 6 a) shows the conductivity between 450 °C and 750 °C at $pO_2 = 10^{-5}$ atm. Interestingly, the conductivity was altered in a temperature-dependent manner. The conductivity of $Bi_4Ti_3O_{12}$ under $pO_2 = 10^{-8}$ atm is shown in Fig. 6 b). A similar conductivity behavior was observed at $pO_2 = 10^{-5}$ atm and 10^{-8} atm; however, at the end of heating process, an increase in pO_2 (10^{-5} atm) generates higher conductivity values.

Table 2 shows the electrical conductivity values at various temperatures and oxygen partial pressures. Although the electrical conductivity increased with rising temperature during the heating process at both partial oxygen pressures, optimal values were obtained at $pO_2 = 10^{-5}$ atm. On the other hand, the decline in conductivity was lower at $pO_2 = 10^{-5}$ atm than at 10^{-8} atm. Upon reaching 750 °C at both working pressures, the material was maintained at this temperature for 10 min. Subsequently, the electrical conductivity was re-estimated before initiating the cooling process. At this stage, the conductivity values decreased by 35.95 % and 45.01 % for $pO_2 = 10^{-5}$ atm and 10^{-8} atm, respectively. Changes in electrical properties has been studied by different authors, such as Jiménez et al. who studied the electrical and piezoelectric properties of a doped bismuth titanate. The results showed that the electrical conductivity followed an Arrhenius plot at different heating and cooling temperatures, indicating that the dielectric and electrical properties were affected by point defects [34].

As observed in Fig. 6, the conductivity is decreased with reduced oxygen partial pressure; this phenomenon is controlled by holes. The Brouwer diagrams for $Bi_4Ti_3O_{12}$ show that the point at which the concentrations of electrons and holes are equal (n = p) mark the point that separates the reduction zone from the oxidation zone. In the reduction zone, the free electrons carry the prevailing charge, whereas the holes carry the prevailing charge in the oxidation zone [28]. $Bi_4Ti_3O_{12}$ is a strongly oxidized material with p-type character as reported previously [28,52–54]. Moreover, the holes control the conductivity even at high oxygen concentrations and bismuth vacancies. The oxygen vacancy concentration must be increased using an optimal dopant for ionic conduction applications.

The conductivity results shown in Fig. 6 present three zones with different slopes that can be used to calculate the activation energies for freeing charge carriers on the conductivity and temperature plot corresponding to the Arrhenius-type behavior pattern [34–36]. Arrhenius provided a mathematical representation for thermally activated processes that establishes the rate at which a process occurs within a particular temperature. The dependence is exponential and parameterized by the energy, which can be thought of as the "activation energy" [55]. Thus, the slopes can be calculated corresponding to the bismuth titanate activation energies under the experimental conditions reported in the present study, according to the following equation:

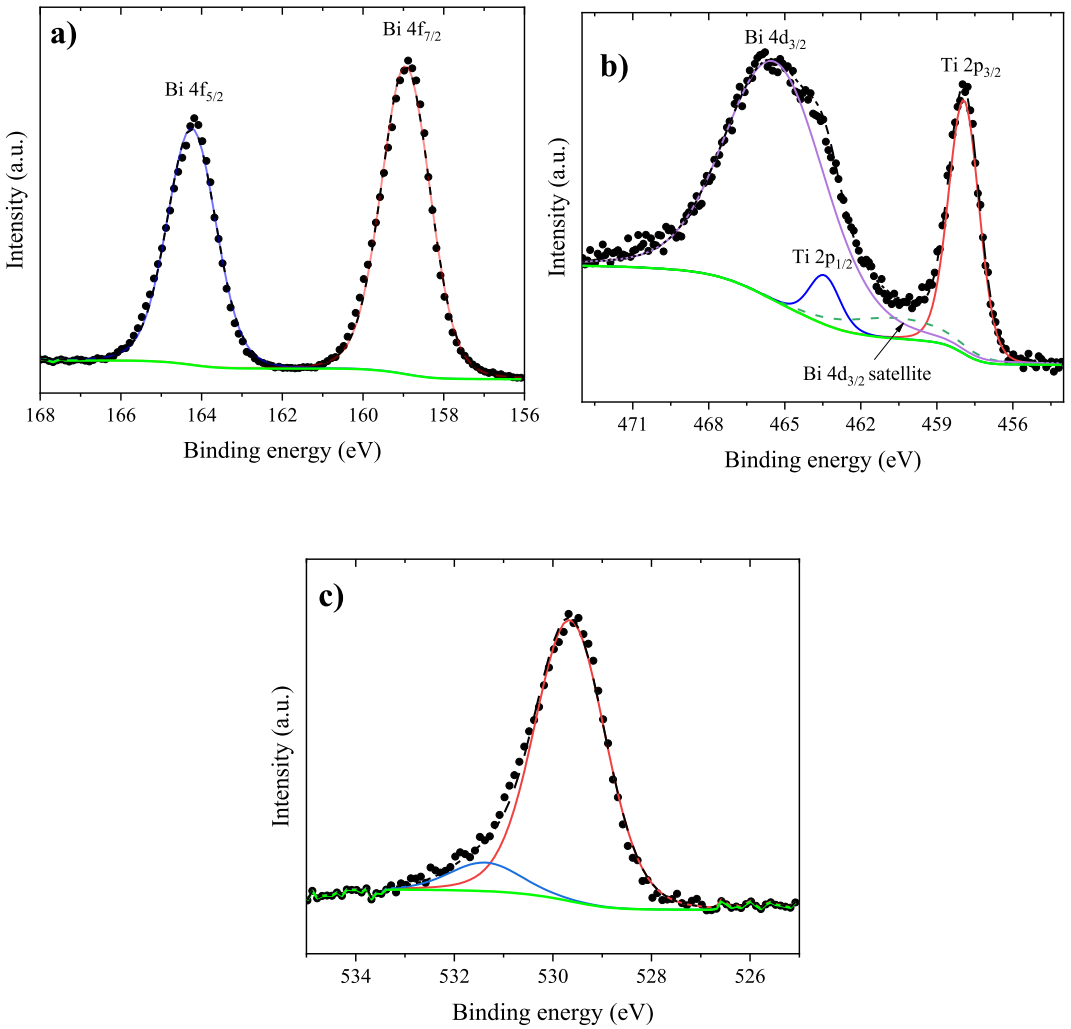

Fig. 5. XPS high-resolution spectra of $Bi_4Ti_3O_{12}$: a) Bi 4f, b) Ti 2p, Bi 4d, and c) O1s.

Table 1
Core level binding energies and full width half maximums of $Bi_4Ti_3O_{12}$.

	Bi 4f		Ti 2p		Bi 4d	O 1s	
	7/2	5/2	3/2	1/2	3/2	(1)	(2)
Binding Energy (eV)	159.0	164.2	458.0	463.6	465.6	529.6	531.4
FWHM (eV)	1.4	1.4	1.4	1.4	4.6	1.7	1.7

$$\sigma = \exp\left(\frac{-E_a}{kT}\right) \tag{1}$$

The activation energy at $pO_2 = 10^{-5}$ atm and temperature interval ranging from 450 °C to 570 °C was 0.81 eV, while that at $pO_2 = 10^{-8}$ atm from 450 °C to 600 °C was 0.79 eV. The low activation energy values indicate that the conduction mechanism could be attributed to the mobility of point defects formed by holes [35]. At intermediate temperatures and $pO_2 = 10^{-5}$ atm, the activation energy was 4.67 eV, while at $pO_2 = 10^{-8}$ atm, it was 4.32 eV. Within this temperature interval, the conduction mechanism was associated with the mobility of holes and vacancies [24,35]. Finally, at higher temperature and $pO_2 = 10^{-5}$atm, the activation energy was 1.18 eV and at $pO_2 = 10^{-8}$ atm, it was 0.90 eV. Under these conditions, the conduction mechanisms are attributed to the combination of the mobility of holes, vacancies and ionization enthalpy [24,34,36]. The reduction in activation energy values with respect to intermediate temperatures was because there was no morphological change. These results agree with the work of other authors who evaluated bismuth titanate without pressure control [24,34,36].

Fig. 7 a) is a schematic of the movement in the octahedral conformation of the $Bi_4Ti_3O_{12}$ structure due to the temperature increase

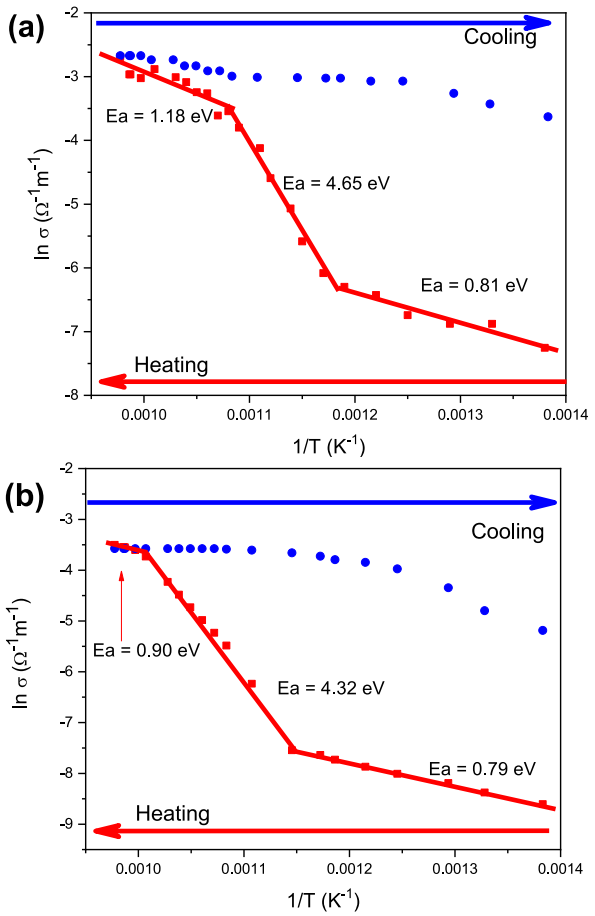

Fig. 6. Electrical conductivity of $Bi_4Ti_3O_{12}$ in a temperature range from 450 °C to 750 °C: a) $pO_2 = 10^{-5}$ atm and b) $pO_2 = 10^{-8}$ atm.

Table 2
Electrical conductivity of $Bi_4Ti_3O_{12}$ sample during heating and cooling processes.

pO_2 (atm)	Conductivity ln σ ($\Omega^{-1}m^{-1}$)			
	450 °C	600 °C	750 °C	
	Heating			Increase (%)
$\mathbf{1\times10^{-5}}$	−7.25	−5.07	−2.69	62.90
$\mathbf{1\times10^{-8}}$	−8.61	−3.01	−3.50	59.33
		Cooling		Decrease (%)
$\mathbf{1\times10^{-5}}$	−2.67	−3.01	−3.63	35.95
$\mathbf{1\times10^{-8}}$	−3.58	−3.61	−5.18	45.01

and point defects formed because of the thermal activation. The low activation energy at the higher temperature is attributed to point defects, such as holes and oxygen vacancies; these defects are affected by increasing temperature. Fig. 7 b) depicts a representation of the behavior of the octahedral structure and involved point defects during cooling process. Due to the slow cooling process, although the conductivity decreased, it was not as significant: for the system at oxygen partial pressure of 10^{-5} and 10^{-8} atm the conductivity reduction was 35.95 and 45.01 %, respectively. During the cooling process, the material changes are related to the decrease in oxygen vacancies and holes, however, because the partial pressure of oxygen is constant, the mechanism of relocation of oxygen atoms is favored and since the temperature gradually decreases, it allows a greater balance to be reached in the concentration of point defects, so the conductivity decreases, but without returning to the initial value (conductivity before heating). It is worth mentioning that according to the XPS and XRD results, the structural modifications are not related to phase changes, but to a preferential orientation and crystal growth.

The increase in the conductivity of $Bi_4Ti_3O_{12}$ was attributed to the presence of point defects, which cause structural changes such as crystal lattice distortion [56]. Additionally, the slow heating and cooling process of 10 °C/min, as well as constant oxygen partial pressure, caused the concentration of point defects to reach equilibrium [26,57]. Despite the scientific contributions in this topic, there

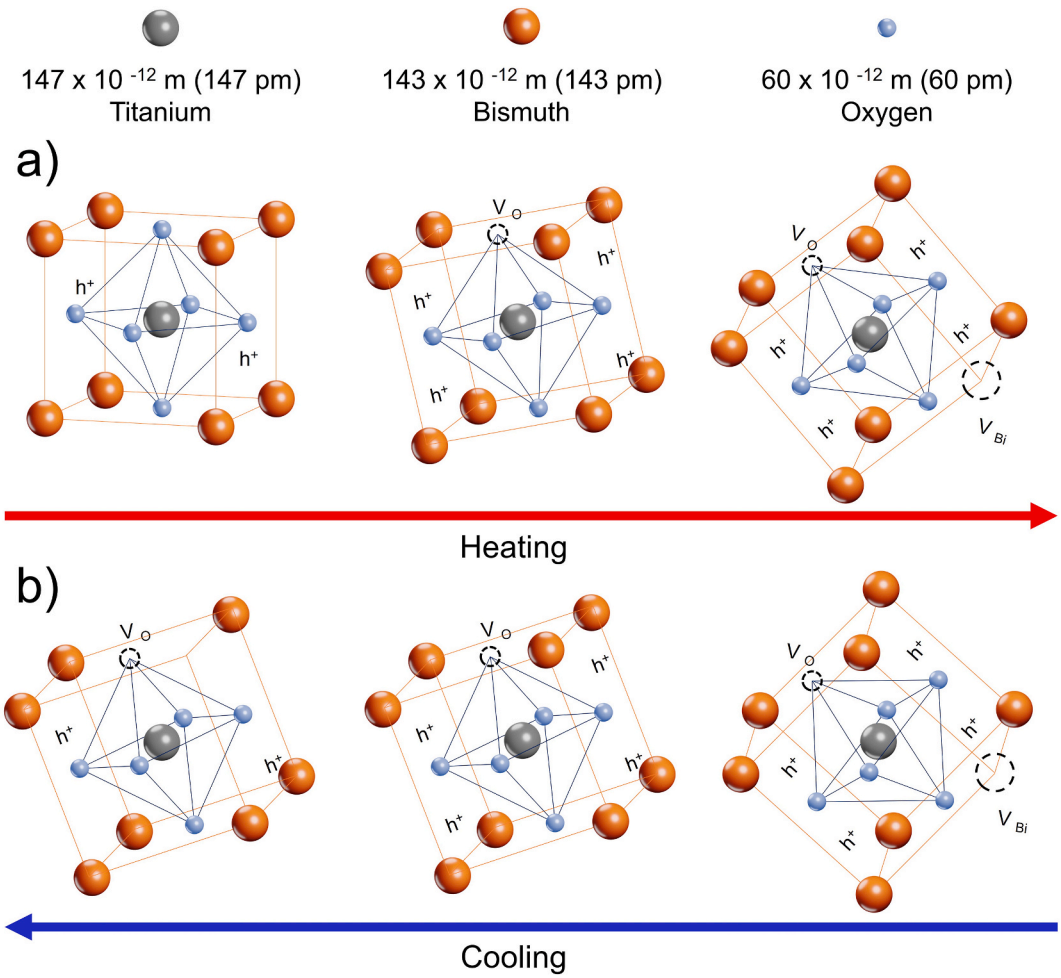

Fig. 7. Representation of the structural movement and $Bi_4Ti_3O_{12}$ point defects due to the thermal activation during the heating and cooling processes.

is still a wide area of opportunity in the implementation of new methods and tools developed to characterize point defects in the crystal lattice of ceramic materials, which would allow introducing, optimizing, concentrating and distributing point defects for specific purposes [57,58].

4. Conclusions

The analysis of the electrical conductivity of $Bi_4Ti_3O_{12}$ at $pO_2 = 10^{-5}$ and $pO_2 = 10^{-8}$ atm revealed that higher conductivity was obtained at higher oxygen partial pressure, which increased further in a temperature-dependent manner. The activation energies were associated with the mobility of holes and bismuth vacancies. Nevertheless, the conductivity was mediated by holes even in the presence of mobility of bismuth and oxygen vacancies; thus, the mobility of oxygen vacancies must be increased for ionic conduction applications. Finally, the electrical conductivity value of $Bi_4Ti_3O_{12}$ was improved compared to the initial value and was preserved during the cooling process due to the gradual heating and slow cooling. The increase in temperature from 450 °C to 750 °C at $pO_2 = 10^{-5}$ atm increased the electrical conductivity by about 62.9 %, whereas the decrease in temperature from 750 °C to 450 °C reduced the electrical conductivity by 35.95 %. Taken together, the enhanced conductivity in the present study was attributed to the structure changes generated by the point defects and the gradual heating and slow cooling processes.

CRediT authorship contribution statement

Carmen Martínez-Morales: Writing – original draft, Methodology, Investigation, Formal analysis, Conceptualization. **Paulina Arellanes-Lozada:** Visualization, Formal analysis, Data curation. **Josué López Rodríguez:** Visualization, Supervision, Formal analysis. **Antonio Romero-Serrano:** Validation, Supervision, Project administration. **D. González-García:** Visualization, Formal analysis.

Declaration of competing interest

The authors declare that they have no known competing financial interests or personal relationships that could have appeared to influence the work reported in this paper.

Acknowledgments

The authors thank the National Council Humanities for Science and Technology (CONAHCYT) and National Polytechnic Institute (IPN) for supporting this research.

References

[1] M. Mostafa, Z.A. Alrowaili, G.M. Rashwan, M.K. Gerges, Ferroelectric behavior and spectroscopic properties of La-Modified lead titanate nanoparticles prepared by a sol-gel method, Heliyon 6 (2020) e03389.
[2] M. Kumar, D.M. Phase, R.J. Choudhary, Structural, ferroelectric and dielectric properties of multiferroic YMnO3 synthesized via microwave assisted radiant hybrid sintering, Heliyon 5 (2019) e01691.
[3] E.H. Yahakoub, A. Bendahhou, I. Jalafi, F. Chaou, S. El Barkany, Z. Bahari, M. Abou-Salama, Effect of sodium substitution by yttrium on the structural, dielectric and electrical properties of Ba2Na(1-3x)YxNb5O15 ceramics, Heliyon 9 (2023) e21037.
[4] S. Xie, Z. Tan, L. Jiang, R. Nie, Q. Xu, Y. Chen, J. Zhu, Q. Wang, Ferroelastic properties and compressive stress-strain response of bismuth titanate based ferroelectrics, Ceram. Int. 46 (2020) 1183–1188.
[5] C. Săvescu, D. Comeagă, A. Stoicescu, Optimization of cantilever piezoelectric harvester to triangular shape with material reduction using finite element analysis, Heliyon 10 (2024) e33209.
[6] S. Mahboubizadeh, S.T. Dilamani, S. Baghshahi, Piezoelectricity performance and β-phase analysis of PVDF composite fibers with BaTiO3 and PZT reinforcement, Heliyon 10 (2024) e25021.
[7] M. Barsoum, Fundamentals of Ceramics, Inst. Physics Publising, Philadelphia, 2003.
[8] A. Singh, S. Monga, N. Sharma, K. Sreenivas, R.S. Katiyar, Ferroelectric, piezoelectric mechanism and applications, J. Asían Ceram. Soc. 10 (2022) 275–291.
[9] V.A. Isupov, Systematization of Aurivillius-type layered oxides, Inorg. Mater. 42 (2006) 1094–1098.
[10] S.A. Ivanov, T. Sarkar, E.A. Fortalnova, E.D. Politova, S.Y. Stefanovich, M.G. Safronenko, P. Nordblad, R. Mathieu, Composition dependence of the multifunctional properties of Nd-doped Bi 4 Ti 3 O 12 ceramics, J. Mater. Sci. Mater. Electron. 28 (2017) 7692–7707.
[11] K. Wang, Z. Guan, X. Liang, S. Song, P. Lu, C. Zhao, L. Yue, Z. Zeng, Y. Wu, Y. He, Remarkably enhanced catalytic performance in CoO(x)/Bi(4)Ti(3)O(12) heterostructures for methyl orange degradation via piezocatalysis and piezo-photocatalysis, Ultrason. Sonochem. 100 (2023) 106616.
[12] T. Jardiel, A.C. Caballero, M. Villegas, Electrical properties in WO3 doped Bi4Ti3O12 materials, J. Eur. Ceram. Soc. 27 (2007) 4115–4119.
[13] S. Li, J. Liu, T. Guo, W. Dong, K. Bi, Y. Luo, Piezoelectricity and flexoelectricity of sodium bismuth titanate-based ceramics, Ceram. Int. 46 (2020) 2049–2054.
[14] M.-Q. Cai, Z. Yin, M.-S. Zhang, Y.-Z. Li, First-principles study of ferroelectric and nonlinear optical property in bismuth titanate, Chem. Phys. Lett. 401 (2005) 405–409.
[15] A. Kumar, P. Sharma, T. Wang, C.W. Lai, G. Sharma, P. Dhiman, Recent progresses in improving the photocatalytic potential of Bi4Ti3O12 as emerging material for environmental and energy applications, J. Ind. Eng. Chem. 138 (2024) 1–16.
[16] J. Zhang, L. Ma, H. Gu, W. Xia, J. He, H. Sun, J. Liu, Photocatalytic performance of Au/Bi4Ti3O12 composite improved by synergistic piezoelectric effect and exciton-plasmon, Ceram. Int. 50 (2024) 27984–27994.
[17] J.D. Bobić, M.M. Vijatović Petrović, J. Banys, B.D. Stojanović, Electrical properties of niobium doped barium bismuth-titanate ceramics, Mater. Res. Bull. 47 (2012) 1874–1880.
[18] O. Subohi, G.S. Kumar, M.M. Malik, R. Kurchania, Synthesis of bismuth titanate with urea as fuel by solution combustion route and its dielectric and ferroelectric properties, Optik 125 (2014) 820–823.
[19] P. Fang, H. Fan, Z. Xi, W. Chen, Studies of structural and electrical properties on four-layers Aurivillius phase BaBi4Ti4O15, Solid State Commun. 152 (2012) 979–983.
[20] J.D. Bobić, M.M. Vijatović, S. Greičius, J. Banys, B.D. Stojanović, Dielectric and relaxor behavior of BaBi4Ti4O15 ceramics, J. Alloys Compd. 499 (2010) 221–226.
[21] J.O. Herrera Robles, C.A. Rodríguez González, S.D. de la Torre, L.E. Fuentes Cobas, P.E. García Casillas, H. Camacho Montes, Dielectric properties of bismuth titanate densified by spark plasma sintering and pressureless sintering, J. Alloys Compd. 536 (2012) S511–S515.
[22] M. Takahashi, Y. Noguchi, M. Miyayama, Electrical conduction mechanism in Bi4Ti3O12 single crystal, Jpn. J. Appl. Phys. 41 (2002) 7053–7056.
[23] M. Takahashi, Estimation of ionic and hole conductivity in bismuth titanate polycrystals at high temperatures, Solid State Ionics 172 (2004) 325–329.
[24] Y.-G. Jeong, G.-J. Lee, S.-H. Lee, H.-S. Ma, B.-H. Kim, K.-H. Park, J.-J. Park, K. Lee, M.-K. Lee, Piezoelectricity, thermal stability, and fatigue resistance in Nb and Ta-doped Bi4Ti3O12 high-temperature piezoceramics, Ceram. Int. 48 (2022) 12764–12771.
[25] M. Yıldırım, Current conduction and steady-state photoconductivity in photodiodes with bismuth titanate interlayer, Thin Solid Films 615 (2016) 300–304.
[26] M.-Q. Cai, Z. Yin, M.-S. Zhang, Y.-Z. Li, Electronic structure of the ferroelectric-layered perovskite bismuth titanate by ab initio calculation within density functional theory, Chem. Phys. Lett. 399 (2004) 89–93.
[27] D.P.C. Shih, A. Aguadero, S.J. Skinner, A-site acceptor-doping strategy to enhance oxygen transport in sodium–bismuth–titanate perovskite, J. Am. Ceram. Soc. 106 (2023) 100–108.
[28] M.d.C. Martínez-Morales, J.A. Romero-Serrano, C. Gómez-Yáñez, L.L. Rojas, Approximations to defect chemistry in Bi4Ti3O12, Funct. Mater. Lett. 9 (2016) 1642006.
[29] S. Lanfredi, M.A.L. Nobre, Conductivity mechanism analysis at high temperature in bismuth titanate: a single crystal with sillenite-type structure, Appl. Phys. Lett. 86 (2005).
[30] Y. Liu, Y. Pu, Z. Sun, Correlation between lattice distortion and magnetic and electrical properties of Fe-doped Bi4Ti3O12 ceramics, J. Mater. Sci. Mater. Electron. 26 (2015) 7484–7489.
[31] M. Takahashi, Y. Noguchi, M. Miyayama, Electrical conduction mechanism in Bi4Ti3O12 single crystal, Jpn. J. Appl. Phys. 41 (2002) 7053.
[32] M. Takahashi, Y. Noguchi, M. Miyayama, Effects of V-doping on mixed conduction properties of bismuth titanate single crystals, Jpn. J. Appl. Phys. 42 (2003) 6222.
[33] M. Miyayama, Y. Noguchi, M. Takahashi, Electrical conduction properties of La-substituted bismuth titanate single crystals, J. Ceram. Process. Res. 6 (2005) 281–285.
[34] B. Jiménez, A. Castro, L. Pardo, P. Millán, R. Jiménez, Electric and ferro-piezoelectric properties of (SBN)1−x(BTN)x ceramics obtained from amorphous precursors, J. Phys. Chem. Solids 62 (2001) 951–958.
[35] H.S. Shulman, M. Testorf, D. Damjanovic, N. Setter, Microstructure, electrical conductivity, and piezoelectric properties of bismuth titanate, J. Am. Ceram. Soc. 79 (1996) 3124–3128.
[36] S.H. Ng, J. Xue, J. Wang, Bismuth titanate from mechanical activation of a chemically coprecipitated precursor, J. Am. Ceram. Soc. 85 (2002) 2660–2665.
[37] F. Ambriz-Vargas, R. Zamorano-Ulloa, A. Romero-Serrano, J. Ortiz-Landeros, J. Crespo-Villegas, D. Ramírez-Rosales, C. Gómez-Yáñez, Point-defect chemistry on the polarization behavior of niobium doped bismuth titanate, J. Mex. Chem. Soc. 61 (2017) 317–325.

[38] R.C. Oliveira, L.S. Cavalcante, J.C. Sczancoski, E.C. Aguiar, J.W.M. Espinosa, J.A. Varela, P.S. Pizani, E. Longo, Synthesis and photoluminescence behavior of Bi4Ti3O12 powders obtained by the complex polymerization method, J. Alloys Compd. 478 (2009) 661–670.
[39] J. Lopez-Martinez, A. Romero-Serrano, A. Hernandez-Ramirez, B. Zeifert, C. Gomez-Yañez, R. Martinez-Sanchez, Thermal analysis and prediction of phase equilibria in the TiO2–Bi2O3 system, Thermochim. Acta 516 (2011) 35–39.
[40] A. Saini, R. Kumar, R. Kumar, Introduction and brief history of thermoelectric materials, in: R. Kumar, R. Singh (Eds.), Thermoelectr. Adv. Thermoelectr. Mater., Woodhead Publishing, 2021, pp. 1–19.
[41] J.C. Rocha Hoyos, E.A. Llanes Cedeño Semiconductores, Conceptos y aplicaciones, Una revisión bibliográfica, E-IDEA 4.0 Revista Multidisciplinar 2 (2020) 12–26.
[42] A. Watcharapasorn, P. Siriprapa, S. Jiansirisomboon, Grain growth behavior in bismuth titanate-based ceramics, J. Eur. Ceram. Soc. 30 (2010) 87–93.
[43] J.S. Patwardhan, M.N. Rahaman, Compositional effects on densification and microstructural evolution of bismuth titanate, J. Mater. Sci. 39 (2004) 133–139.
[44] T. Kimura, T. Yoshimoto, N. Iida, Y. Fujita, T. Yamaguchi, Mechanism of grain orientation during hot-pressing of bismuth titanate, J. Am. Ceram. Soc. 72 (1989) 85–89.
[45] Z. Xie, X. Tang, J. Shi, Y. Wang, G. Yuan, J.-M. Liu, Excellent piezo-photocatalytic performance of Bi4Ti3O12 nanoplates synthesized by molten-salt method, Nano Energy 98 (2022) 107247.
[46] F.E. Oropeza, I.J. Villar-Garcia, R.G. Palgrave, D.J. Payne, A solution chemistry approach to epitaxial growth and stabilisation of Bi2Ti2O7 films, J. Mater. Chem. A 2 (2014) 18241–18245.
[47] E.V. Ramana, N.V. Prasad, D.M. Tobaldi, J. Zavašnik, M.K. Singh, M.J. Hortigüela, M.P. Seabra, G. Prasad, M.A. Valente, Effect of samarium and vanadium co-doping on structure, ferroelectric and photocatalytic properties of bismuth titanate, RSC Adv. 7 (2017) 9680–9692.
[48] M. Murugesan, S.R. Meher, TiO2-ZnO Composite thin films fabricated by Sol-Gel spin coating for room temperature impedometric acetone sensing, Sens. Actuators, A 369 (2024) 115181.
[49] L. Wang, W. Ma, Y. Fang, Y. Zhang, M. Jia, R. Li, Y. Huang, Bi4Ti3O12 synthesized by high temperature solid phase method and it's visible catalytic activity, Procedia Environ. Sci. 18 (2013) 547–558.
[50] Č. Jovalekić, M. Zdujić, L. Atanasoska, Surface analysis of bismuth titanate by Auger and X-ray photoelectron spectroscopy, J. Alloys Compd. 469 (2009) 441–444.
[51] A.A. Roselin, R. Karkuzhali, N. Anandhan, G. Gopu, Bismuth titanate (Bi4Ti3O12, BTO) sol–gel spin coated thin film for heavy metal ion detection, J. Mater. Sci. Mater. Electron. 32 (2021) 24801–24811.
[52] M. Takahashi, Y. Noguchi, M. Miyayama, Estimation of ionic and hole conductivity in bismuth titanate polycrystals at high temperatures, Solid State Ionics 172 (2004) 325–329.
[53] H. Katsu, Crystal-and defect-chemistry of fine grained thermistor ceramics on BaTiO3 basis with BaO-excess, Elektronische Materialien (2011).
[54] W. Preis, W. Sitte, Electronic conductivity and chemical diffusion in n-conducting barium titanate ceramics at high temperatures, Solid State Ionics 177 (2006) 3093–3098.
[55] C.R.M. Grovenor, in: C.R.M. Grovenor (Ed.), Microelectronic Materials, Taylor and Francis Group, 1989, p. 544.
[56] Y. Chen, J. Xu, S. Xie, Z. Tan, R. Nie, Z. Guan, Q. Wang, J. Zhu, Ion doping effects on the lattice distortion and interlayer mismatch of aurivillius-type bismuth titanate compounds, Materials 11 (2018) 821.
[57] S. Jayashree, M. Ashokkumar, Switchable intrinsic defect chemistry of titania for catalytic applications, Catalysts 8 (2018) 601.
[58] C. Ricca, U. Aschauer, Mechanisms for point defect-induced functionality in complex perovskite oxides, Appl. Phys. A: Mater. Sci. Process. 128 (2022) 1083.